Autonomous Chemotactic Light-Emitting Swimmers with Trajectories of Increasing Complexity

Ileana-Alexandra Pavel, Gerardo Salinas, Adeline Perro, Alexander Kuhn

COMMUNICATION

**ADVANCED
INTELLIGENT
SYSTEMS**
Open Access

www.advintellsyst.com

Autonomous Chemotactic Light-Emitting Swimmers with Trajectories of Increasing Complexity

Ileana-Alexandra Pavel, Gerardo Salinas, Adeline Perro, and Alexander Kuhn*

Miniaturized autonomous swimmers have become more and more important in many areas of research due to various fields of use, ranging from biomedical to environmental tasks. Precise and predictable control of their trajectories is a key ingredient for increasing their application potential. This can be typically achieved by using external forces such as magnetic or electric fields. An interesting alternative is to use intrinsic features of the swimmers, which allow them to exhibit chemotaxis. Such a built-in "intelligence" enables more complex trajectories, relying on mechanisms that can be considered very basic analogs of decision-making processes. Herein, autonomous light-emitting chemoelectronic swimmers are presented that are able to navigate along trajectories with increasing complexity. Their decision-making capacities are characterized by recording the light emitted along their path by a fully integrated light-emitting diode. Chemotaxis is found to be the main driving force behind their behavior, allowing envisioning such systems for solving complex maze patterns.

Defining the intelligence of artificial systems remains a challenge for the scientific community. A system can eventually show signs of a kind of intelligence if it reacts to a stimulus. For example, Sanchez's group defines the intelligence of nanosystems as their response, e.g., active navigation, to external impulses or to endogenous stimuli.[1] Micro and nanodevices showing such active and adjustable navigation have gained considerable attention, as the propulsion mechanisms are now better understood, and different sophisticated designs have been realized. This is leading to an increase in the number of potential applications, e.g., sensing and bio-sensing,[2] biomedicine,[3,4] imaging,[1] cargo manipulation and delivery,[5] and environmental remediation.[6] The swimmer motion is essentially based on two main types of propulsion: self-propulsion, by either phoretic motion or bubble propulsion, and nonautonomous propulsion, which requires an external source of energy/stimuli.[7–10] Directional motion control of these swimmers in order to

perform interesting and complex tasks remains a challenge.[5,11–13]

In this context, finding the way through a maze is a challenging scientific problem which requires decision-making. Although external energy, in the form of electric[14–16] and magnetic fields (e.g., in an autonomous navigation system controlled by artificial intelligence[17] or in a teleoperation system controlled by a human[18]) or acoustic waves,[19] can allow controlling the motion of motors through different maze structures, it is desirable to develop autonomous swimmers, able to adjust their own trajectory, based on the collection of information from the surrounding medium. Maze solving has been previously studied with various systems, based on Marangoni flow of dye particles,[20] organic droplets,[21–23] inorganic capsules,[24] phenol red dye particles,[25] as well as living organisms such as slime mold[26] and cells.[27] Tracking of such systems as a function of time can be facilitated if they are simultaneously emitting light.

The different approaches for designing light-emitting dynamic systems, based on fluorescence,[28,29] chemiluminescence,[30] (electro)chemiluminescence,[31] or microelectronics,[32] have been recently summarized.[33] Among the various approaches, the use of light-emitting diodes (LEDs) as active ingredients is a very versatile concept to generate motion,[32] for remote steering[34] or for pumping and mixing of liquids in the presence of AC electric fields.[35] With a similar philosophy, light-emitting crawlers have been prepared by functionalizing micro-LEDs with conducting polymers[36] and by using IR-LEDs integrated in a polymeric structure, presenting controlled motion and actuation.[37] However, all these systems require an input of external electric energy to propel or switch on the device.
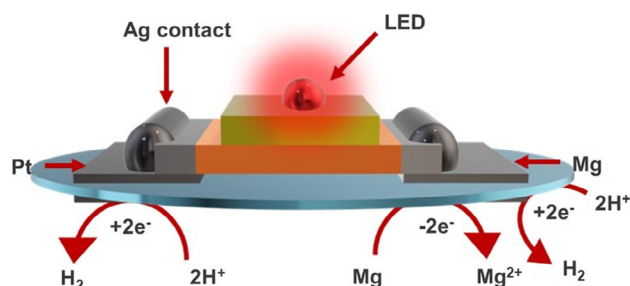
Here we present a LED-based swimmer that not only does not need an external energy input, but is also able to change the direction of its movement in response to a complex chemical gradient. The electronic swimmer, designed by combining small Pt and Mg foil segments with a micro-LED (**Scheme 1** and Figure S1, Supporting Information), presents chemotaxis and magnetotaxis.[38] Chemotaxis is a directed motion in the concentration gradient of a chemical species,[39] whereas magnetotaxis is an oriented movement following an artificial or the terrestrial magnetic field.[40] In the current case, the swimmer shows pronounced chemotaxis, combined with light emission, due to the controlled corrosion of Mg in a H_3O^+ gradient. Magnetotaxis, triggered by the terrestrial magnetic field, is in principle also possible due to the presence of an intrinsic

Dr. I.-A. Pavel, Dr. G. Salinas, Dr. A. Perro, Prof. A. Kuhn
University of Bordeaux, CNRS, Bordeaux INP, ISM, UMR 5255
F-33607 Pessac, France
E-mail: kuhn@enscbp.fr

The ORCID identification number(s) for the author(s) of this article can be found under https://doi.org/10.1002/aisy.202000217.

**ADVANCED
SCIENCE NEWS**

www.advancedsciencenews.com

**ADVANCED
INTELLIGENT
SYSTEMS**
Open Access

www.advintellsyst.com

Scheme 1. Schematic illustration of the chemoelectronic swimmer and the associated chemical reactions occurring at the air/water interface, constituting its driving force.

magnetic moment, originating from the LED components, as has been shown previously.[38] However, in the study reported here the chemical gradients were chosen to be rather strong to facilitate the movement of the relatively bulky and heavy swimmer and to neglect the magnetotaxis effect in all experiments. This does not exclude real applications, including in biomedia, because similar, but considerably smaller swimmers, which are currently under investigation, show motion already for much smaller pH gradients.

To test the behavior of such a chemoelectronic swimmer, its motion was evaluated in channel patterns with different geometric constraints of increasing complexity, representing the building units of a maze. As this is a first proof-of-principle study, the studied maze patterns have a moderate degree of complexity compared to other reported maze-type structures, but they represent the most fundamental and important features that can be encountered in a maze. The swimmer motion was recorded both in daylight and in the dark to monitor the movement and intensity of light emission, respectively.

The simplest arrangement, in which the decision-making capacities can be tested in a dynamically changing environment, is generated by a Y-shaped setup. In this case, the swimmer has the choice between two pathways, leading to a left–right answer. The swimmer is placed at the air/water interface of a 0.125 m$_M$ sodium dodecyl sulfate (SDS) solution, at a distance of ≈3 cm from the tail of the Y structure. An acid gradient is generated, alternatively from the right or left side of the Y setup, by adding a 1.5 M H_2SO_4/SDS solution at a rate of 7.5 mL h^{-1}.

When acid is added from the upper left branch of the Y structure, a homogeneous pH gradient builds up in the cell, as revealed by a pH indicator (**Figure 1**a). Initially this does not seem to affect the swimmer; actually, it tends at the very beginning even to move slightly to the right as can be seen from the daylight image in Figure S2a, Supporting Information. As the pH slowly decreases, the swimmer makes a decision and orients itself toward the ∇pH. Simultaneously, it starts emitting light and follows a quite linear trajectory parallel to the wall of the Y (Figure 1b and Video S1, Supporting Information) with an average speed of 0.19 body lengths per second, which corresponds to an absolute velocity of around 0.9 mm s^{-1}. Only very close to the end it clearly changes direction again to be oriented toward the point of acid injection. When acid is added from the upper right part of the Y, the swimmer shows the opposite behavior (Figure S2b, Supporting Information). Again, when the swimmer reaches a slightly higher proton concentration, light emission starts and its trajectory and speed (0.12 body lengths per second) can also be tracked in the dark (Figure 1c and Video S2, Supporting Information). In both cases, this is because it is necessary to reach a certain proton concentration threshold to provide enough driving force for reducing protons not only directly on the magnesium surface, but also at the platinum site (Scheme 1). At this moment, electrons are transferred through the LED, leading to its illumination. This is also confirmed by the progressive increase of the potential difference between the Mg and Pt electrodes, obtained at different pH values (Figure S3, Supporting Information).

In this initial experiment, the trajectory can be divided into two distinct segments. First, repulsion from the walls due to surface tension effects, combined with the ∇pH, forces the swimmer to follow the contour of the Y structure in a quasi-linear way. In a second segment, when the device is approaching the acid source, it encounters the steepest concentration gradient and therefore reorients, accompanied by a significant increase in light intensity. Both experiments demonstrate that the swimmer can sense its environment, the topography of the walls and the ∇pH and acts accordingly. To further investigate their decision-making capacity, the swimmers were exposed to a sequence of choices in more complex set-ups. A double L structure and a double Y structure were chosen as representative building blocks of a maze.

Figure 1. a) ∇pH revealed by a universal pH indicator 30 s after the beginning of acid injection from the upper left corner. b) Trajectory of the light-emitting swimmer recorded in the dark in the presence of a ∇pH originating from the upper left corner. c) Same as (b) but with acid injection from the upper right corner. The green dot represents the source of acid; the color scale codes the light intensity and a swimmer symbol is positioned at the initial launching location.

Two L-shaped walls were combined with a third long wall to increase the complexity of the setup and the spatial ∇pH profile (Figure S4a, Supporting Information). In this double L setup, the swimmer is placed at the position indicated in Figure S4b, Supporting Information, at the air/water interface of a 0.25 mM SDS solution. The acid gradient is generated by adding a solution of 1 M H_2SO_4/SDS at a rate of 5 mL h^{-1} from the upper left corner of the grid. In this setup, the swimmer must make two sequential left/right decisions to avoid dead ends and has to enter the confined space between two walls (4 cm separation) on the way toward higher acid concentrations.

When acid is added, a front of low pH is reaching the swimmer. Initially, the chemoelectronic device is moving in the same direction as the acid flow due to hydrodynamics. However, as the proton concentration slowly increases, the swimmer changes direction and moves toward the steeper chemical gradient (Figure S4b, Supporting Information). This behavior can be attributed to the swimmer's capacity to sense the confinement imposed by the surrounding structures. In the presence of a very low concentration of acid, hydrodynamics is responsible for the swimmer's motion, as it keeps a certain distance between itself and the walls of the setup. Once the proton concentration increases, the device is able to overcome the hydrodynamic forces and moves straight toward the acid source with an average speed of 0.2 body lengths per second due to its positive chemotactic properties. The higher chemical driving force is again enabling light emission (**Figure 2**a and Video S3, Supporting

Information). At the end of this linear second section, the swimmer faces a new decision and changes its trajectory. It makes a rather abrupt turn to the right with an angle of 140°. As the swimmer reaches a steeper ∇pH, the intensity of emitted light increases until a plateau is reached. As shown in Figure 2a, the swimmer proceeds toward a steeper ∇pH while keeping a maximum distance from both walls. After an additional turn to the left, the chemoelectronic device reaches the highest concentration of acid, also revealed by a maximum light intensity.

Analogously to the double L structure, two Y-shaped walls are positioned in such a way that a smaller open gate (3 cm) is created between them. Combined with an additional long wall (5 cm wide), this constitutes a circuit with a further increased complexity. As in the previous experiments, the swimmer is placed at the air/water interface of a 0.25 mM SDS solution. At the end of the path, a gradient of acid is generated by adding a 1.5 M H_2SO_4/SDS solution with a rate of 7.5 mL h^{-1} (Figure S5a, Supporting Information). In this setup, the swimmer has to evaluate whether it will head toward a dead end or follow the pH gradient. This choice has to be made twice in a row, followed by a decision to enter the gate.

Similar to the LL structure, at low H_3O^+ concentrations, the swimmer moves away from the gradient, pushed by the hydrodynamic flow (Figure S5a, Supporting Information). After this short induction period, the swimmer's symmetry axis aligns with the direction of the ∇pH and starts moving toward the gradient while emitting a low light intensity (Figure 2b and Figure S5b

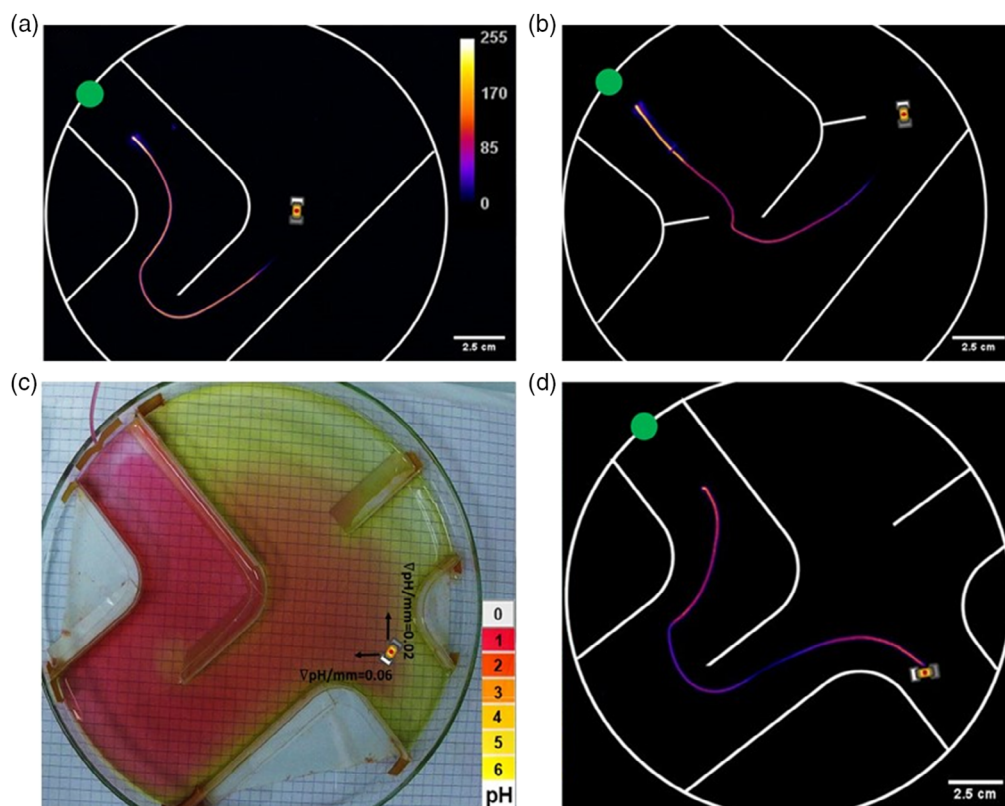**Figure 2.** a) Trajectory of the light-emitting swimmer recorded in the dark in the presence of a ∇pH generated at the upper left corner in a double L setup. b) Same as (a) but in a double-Y-type setup. c) ∇pH revealed by a universal pH indicator 60 s after the beginning of acid injection from the upper left corner, in a maze-type setup. d) Trajectory of the swimmer in setup (c).

**ADVANCED
SCIENCE NEWS**
www.advancedsciencenews.com

**ADVANCED
INTELLIGENT
SYSTEMS**
Open Access

www.advintellsyst.com

and Video S4, Supporting Information). It is remarkable that even slight differences in pH gradient allow this preferential motion. In the current case, at the left side a $\nabla pH\,mm^{-1}$ of ≈ 0.03 is present in the vicinity of the swimmer, whereas $\nabla pH\,mm^{-1} = 0.01$ at its right side, and this difference is enough to trigger a turn toward the left part of the structure. Compared with the movement in the previous setup, the swimmer has a smoother trajectory until it faces the second decision. As the channel is wider, this induces less constraints and consequently the swimmer is not moving completely parallel to the walls but follows the pH gradient. Concomitantly, the LED intensity increases as the swimmer reaches higher H_3O^+ concentrations. Then the second decision, between a dead end and a stronger pH gradient, is made and the autonomous device slowly changes its direction with an angle of $140°$ to follow the ∇pH. When the swimmer arrives in front of the gate, it changes its orientation again rather abruptly. After exiting the gate, it reorientates and continues its trajectory, almost parallel to the walls, toward the source of acid. During the whole journey through the YY structure, the swimmer has an average speed of 0.23 body lengths per second and the light intensity is slowly increasing in agreement with the steady increase of H_3O^+ concentration.

The interplay between the chemotactic behavior and the ability of the swimmer to sense the surrounding topography was finally analyzed in a more complex structure. Starting from the double L setup, new elements were added. A first corridor as the starting point, combined with a path toward a dead end and a gate that leads to an open space, represent the first elements encountered in a typical maze. The swimmer is placed in the extreme lower right corner of the maze, at the air/water interface of a 0.375 mM SDS solution. At the end of the path, formed by the double L, an acid gradient is generated by adding a 1 M H_2SO_4/SDS solution at a rate of 5 mL h^{-1}.

Initially, at low H_3O^+ concentration (Figure 2c) the swimmer feels the proximity of the two walls and tries to stay at some distance while moving in arbitrary directions. When the concentration of acid increases, it makes an almost $180°$ turn around its own axis and orients itself with respect to the chemical gradient (Figure S6, Supporting Information). When the swimmer reaches a higher proton concentration, the intensity of the emitted light starts to increase (Figure 2d and Video S5, Supporting Information). Initially, the trajectory is almost parallel to the walls and the swimmer takes the decision to turn left, around the corner of the structure, despite the fact that there is also some acid present toward the right and ahead of it, as shown in Figure 2c. As in the previous experiments (vide supra), it is again only a rather small difference in pH gradient ($\nabla pH\,mm^{-1} = 0.06$ and 0.02 at the left and right side, respectively), which triggers a turn to the left. As the swimmer enters the corridor, it starts moving toward the acid in a diagonal trajectory until it gets close to the end of the arm of the first L. There, it changes its movement, making the decision not to go toward the dead end but to turn in a half-circle. When the chemoelectronic device enters the corridor formed by the second L, it moves almost parallel to the walls of the corner, which is analogous to the behavior described earlier for the LL structure. However, the absolute light intensity of the swimmer in this setup is lower in comparison with the LL path, using the same concentration and feeding rate of acid. This is because the volume of the solution in the maze-type setup

is slightly higher than in the LL structure, leading to a lower overall $[H_3O^+]$. In the pH visualization experiment (Figure 2c and Video S6, Supporting Information), some patches appear along the gradient due to the less linear hydrodynamics in this more complex pattern. These patches have a higher pH and consequently the intensity of light is lower as the swimmer passes through them. Finally, the device ends up reaching the extremity of the structure where the proton source is located. Due to the complexity of the structure, the swimmer presents speed variations along the path, but the average speed during the overall trajectory is still of the same order of magnitude as for the previous setups (0.18 body lengths per second).

We have demonstrated the apparent "intelligence" of a completely autonomous chemoelectronic swimmer that converts water-born fuel (H^+) into directed motion. The self-propelled device shows controlled movement toward low pH in different setups, illustrating the capacity of decision-making in very simple or more complex structures, representing the basic building blocks of a maze. The motion can be very easily visualized with the help of the concomitant emission of light due to the presence on an integrated miniaturized LED. The driving force produced by the spontaneous redox reactions occurring at both connectors of the LED allows efficient fueling of the electronic component with electrons. Such model devices can help to better understand the sometimes very complex behavior of natural systems and open up interesting perspectives for developing more sophisticated "intelligent" systems. For a better understanding of the cooperative mechanism of natural systems involving several swimmers, new and smaller light-emitting objects are currently under study in our group.

Supporting Information

Supporting Information is available from the Wiley Online Library or from the author.

Conflict of Interest

The authors declare no conflict of interest.

Keywords

autonomous swimmers, chemotaxis, light emission, maze structures

[1] G. T. Van Moolenbroek, T. Patiño, J. Llop, S. Sánchez, *Adv. Intell. Syst.* **2020**, *2*, 2000087.

**ADVANCED
SCIENCE NEWS**

www.advancedsciencenews.com

**ADVANCED
INTELLIGENT
SYSTEMS**
Open Access

www.advintellsyst.com

[2] M. Pacheco, M. Á. López, B. Jurado-Sánchez, A. Escarpa, *Anal. Bioanal. Chem.* **2019**, *411*, 6561.

[3] M. Mathesh, J. Sun, D. A. Wilson, *J. Mater. Chem. B* **2020**, *8*, 7319.

[4] W. Wang, Z. Wu, Q. He, *VIEW* **2020**, *1*, 20200005.

[5] D. Xu, Y. Wang, C. Liang, Y. You, S. Sanchez, X. Ma, *Small* **2020**, *16*, 1902464.

[6] B. Jurado-Sánchez, J. Wang, *Environ. Sci. Nano* **2018**, *5*, 1530.

[7] L. Bouffier, V. Ravaine, N. Sojic, A. Kuhn, *Curr. Opin. Colloid Interface Sci.* **2016**, *21*, 57.

[8] K. Dietrich, N. Jaensson, I. Buttinoni, G. Volpe, L. Isa, *Phys. Rev. Lett.* **2020**, *125*, 098001.

[9] Z. Ye, Y. Sun, H. Zhang, B. Song, B. Dong, *Nanoscale* **2017**, *9*, 18516.

[10] M. Fernández-Medina, M. A. Ramos-Docampo, O. Hovorka, V. Salgueiriño, B. Städler, *Adv. Funct. Mater.* **2020**, *30*, 1908283.

[11] J. Wang, K. M. Manesh, *Small* **2010**, *6*, 338.

[12] W. Z. Teo, M. Pumera, *Chem. Eur. J.* **2016**, *22*, 14796.

[13] Q. Yang, L. Xu, W. Zhong, Q. Yan, Y. Gao, W. Hong, Y. She, G. Yang, *Adv. Intell. Syst.* **2020**, *2*, 2000049.

[14] L. Zhang, Z. Xiao, X. Chen, J. Chen, W. Wang, *ACS Nano* **2019**, *13*, 8842.

[15] E. Miyako, K. Kono, E. Yuba, C. Hosokawa, H. Nagai, Y. Hagihara, *Nat. Commun.* **2012**, *3*, 1226.

[16] A. Adamatzky, A. Chiolerio, K. Szaciłowski, *Soft Matter* **2020**, *16*, 1455.

[17] T. Li, X. Chang, Z. Wu, J. Li, G. Shao, X. Deng, J. Qiu, B. Guo, G. Zhang, Q. He, L. Li, J. Wang, *ACS Nano* **2017**, *11*, 9268.

[18] C. Pacchierotti, V. Magdanz, M. Medina-Sánchez, O. G. Schmidt, D. Prattichizzo, S. Misra, *J. Micro-Bio Robot.* **2015**, *10*, 37.

[19] X. Lu, F. Soto, J. Li, T. Li, Y. Liang, J. Wang, *ACS Appl. Mater. Interfaces* **2017**, *9*, 38870.

[20] K. Suzuno, D. Ueyama, M. Branicki, R. Tóth, A. Braun, I. Lagz, *Langmuir* **2014**, *30*, 9251.

[21] I. Lagzi, S. Soh, P. J. Wesson, K. P. Browne, B. A. Grzybowski, *J. Am. Chem. Soc.* **2010**, *132*, 1198.

[22] J. Čejková, M. Novák, F. Štěpánek, M. M. Hanczyc, *Langmuir* **2014**, *30*, 11937.

[23] C. Jin, C. Krüger, C. C. Maass, *PNAS* **2017**, *114*, 5089.

[24] G. Zhao, M. Pumera, *Lab Chip* **2014**, *14*, 2818.

[25] K. Suzuno, D. Ueyama, M. Branicki, R. Tóth, A. Braun, I. Lagz, *Langmuir* **2014**, *30*, 9251.

[26] A. Adamatzky, *IEEE Trans. Nanobiosci.* **2012**, *11*, 131.

[27] L. Tweedy, P. A. Thomason, P. I. Paschke, K. Martin, L. M. Machesky, M. Zagnoni, R. H. Insall, *Science* **2020**, *369*, eaay9792.

[28] K. Villa, C. L. Manzanares-Palenzuela, Z. Sofer, S. Matějková, M. Pumera, *ACS Nano* **2018**, *12*, 12482.

[29] S. Ni, E. Marini, I. Buttinoni, H. Wolf, L. Isa, *Soft Matter* **2017**, *13*, 4252.

[30] G. Salinas, A. L. Dauphin, S. Voci, L. Bouffier, N. Sojic, A. Kuhn, *Chem. Sci.* **2020**, *11*, 7438.

[31] M. Sentic, G. Loget, D. Manojlovic, A. Kuhn, N. Sojic, *Angew. Chem., Int. Ed.* **2012**, *51*, 11284.

[32] S. T. Chang, V. N. Paunov, D. N. Petsev, O. D. Velev, *Nat. Mater.* **2007**, *6*, 235.

[33] G. Salinas, I.-A. Pavel, N. Sojic, A. Kuhn, *ChemElectroChem* **2020**, *7*, https://doi.org/10.1002/celc.202001104.

[34] R. Sharma, O. D. Velev, *Adv. Funct. Mater.* **2015**, *25*, 5512.

[35] S. T. Chang, E. Beaumont, D. N. Petsev, O. D. Velev, *Lab Chip* **2008**, *8*, 117.

[36] B. Gupta, M. C. Alfonso, L. Zhang, C. Ayela, P. Garrigue, B. Goudeau, A. Kuhn, *ChemPhysChem* **2019**, *20*, 941.

[37] V. K. Bandari, Y. Nan, D. Karnaushenko, Y. Hong, B. Sun, F. Striggow, D. D. Karnaushenko, C. Beker, M. Faghih, M. Medina-Sanchez, F. Zhu, O. G. Schmidt, *Nat. Electron.* **2020**, *3*, 172.

[38] G. Salinas, A. L. Dauphin, C. Colin, E. Villani, S. Arbault, L. Bouffier, A. Kuhn, *Angew. Chem., Int. Ed.* **2020**, *59*, 7508.

[39] M. N. Popescu, W. E. Uspal, C. Bechinger, P. Fischer, *Nano Lett.* **2018**, *18*, 5345.

[40] K. Bente, A. Codutti, F. Bachmann, D. Faivre, *Small* **2018**, *14*, 1704374.

2000217 (5 of 5)